

# Structures and Reaction Pathways in Rhodium(I)-Catalyzed Hydrogenation of Enamides: A Model DFT Study

Clark R. Landis,\* Peter Hilfenhaus, and Steven Feldgus

Contribution from the Department of Chemistry, University of Wisconsin, Madison, Wisconsin 53706

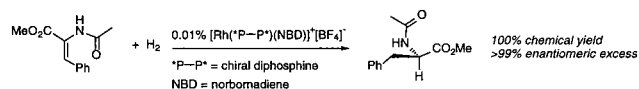
Received May 13, 1999

**Abstract:** The potential energy profile of Rh(I)-catalyzed hydrogenation of enamides has been studied for the simple model system  $[\text{Rh}(\text{PH}_3)_2(\alpha\text{-acetamidoacrylonitrile})]^+$  using a nonlocal density functional method (B3LYP). Intermediates and transition states along four isomeric pathways for dihydrogen activation have been located, and pathways for interconversion between isomeric reaction pathways have been explored. The general sequence of the catalytic cycle involves coordination of  $\text{H}_2$  to  $[\text{Rh}(\text{PH}_3)_2(\alpha\text{-acetamidoacrylonitrile})]^+$  to form a five-coordinate molecular  $\text{H}_2$  complex, followed by oxidative addition of the coordinated molecular hydrogen to form a dihydride complex,  $[\text{RhH}_2(\text{PH}_3)_2(\alpha\text{-acetamidoacrylonitrile})]^+$ . This dihydride is converted into an alkyl hydride by a migratory insertion reaction. Reductive elimination of the hydrogenated acetamidoacrylonitrile completes the catalytic cycle. No computational support for alternate  $\text{H}_2$  activation pathways, such as direct conversion of  $\text{H}_2$  and  $[\text{Rh}(\text{PH}_3)_2(\alpha\text{-acetamidoacrylonitrile})]^+$  to an alkyl hydride, was found. Four isomeric pathways for hydrogenation are followed, corresponding to the four distinct dihydride isomers resulting from cis addition of  $\text{H}_2$  to  $[\text{Rh}(\text{PH}_3)_2(\alpha\text{-acetamidoacrylonitrile})]^+$ . Two of these pathways are excluded from further consideration by virtue of their surprisingly high activation barriers for formation of molecular  $\text{H}_2$  complexes. Of the two pathways with low barriers to formation of dihydride complexes, only one has a sufficiently low barrier for migratory insertion to contribute significantly to catalytic product formation. Overall, we find that formation of a dihydride is endergonic, rapid, and reversible. Migratory insertion to form an alkyl hydride constitutes the turnover-limiting step in the catalytic cycle. This conclusion is supported by comparison of computed and experimental isotope effects in catalytic enamide hydrogenation.

## I. Introduction

The enantioselective, catalytic hydrogenation of enamides is a powerful method for synthesizing chiral amino acids<sup>1–12</sup> and a rich source of mechanistic information concerning selectivity control in catalysis.<sup>13–20</sup> The reaction conditions are mild;

common conditions are 0–50 °C, 0–100 atm  $\text{H}_2$  pressure, and a variety of organic solvents may be used. The overall mechanism as determined for methanol solvent is depicted in Figure 1.<sup>21,22</sup> As shown in Figure 1, the reaction consists of two coupled diastereomeric manifolds (major and minor). The majority (>90%) of the total catalyst accumulates in the major manifold, in the form of  $\mathbf{2}^{\text{maj}}$ . However, by virtue of the much higher reactivity of  $\mathbf{2}^{\text{min}}$  toward  $\text{H}_2$ , virtually all product emanates from the manifold of the minor diastereomer. This mechanistic motif also accounts for the sometimes dramatic effects of temperature,  $\text{H}_2$  pressure, and mass transport on the reaction rates and enantioselectivity.<sup>18,19</sup>



A fundamental understanding of the control of enantioselectivity and activity in a multistep catalytic reaction requires identification of the step, or steps, that limit turnover frequencies and those that fix the product chirality.<sup>23</sup> Given, for example, knowledge of the turnover-limiting step, it is possible, in principle, to create a model transition-state structure and to design rational modifications of the catalyst such that the free energy of activation is lowered. Similarly, given knowledge of

- (1) Knowles, W. S. *Acc. Chem. Res.* **1983**, *16*, 106–112.
- (2) Koenig, K. E. In *Asymmetric Synthesis*; Morrison, J. D., Ed.; Academic Press: Orlando, FL, 1985; Vol. 5.
- (3) Ojima, I. *Catalytic Asymmetric Synthesis*; VCH: New York, 1993.
- (4) Noyori, R. *Acta Chem. Scand.* **1996**, *50*, 380–390.
- (5) Burk, M. J. *J. Am. Chem. Soc.* **1991**, *113*, 8518–8519.
- (6) Burk, M. J.; Gross, M. F.; Harper, T. G. P.; Kalberg, C. S.; Lee, J. R.; Martinez, J. P. *Pure Appl. Chem.* **1996**, *68*, 37–44.
- (7) Ager, D. J.; Fotheringham, I. G.; Laneman, S. A.; Pantaleone, D. P.; Taylor, P. P. *Chim. Oggi-Chem. Today* **1997**, *15*, 11–14.
- (8) Nagel, U.; Albrecht, J. *Topics Catal.* **1998**, *5*, 3–23.
- (9) Kreuzfeld, H. J.; Dobler, C.; Schmidt, U.; Krause, H. W. *Chirality* **1998**, *10*, 535–539.
- (10) Zhu, G. X.; Zhang, X. M. *J. Org. Chem.* **1998**, *63*, 3133–3136.
- (11) Zhu, G. X.; Cao, P.; Jiang, Q. Z.; Zhang, X. M. *J. Am. Chem. Soc.* **1997**, *119*, 1799–1800.
- (12) RajanBabu, T. V.; Ayers, T. A.; Halliday, G. A.; You, K. K.; Calabrese, J. C. *J. Org. Chem.* **1997**, *62*, 6012–6028.
- (13) Halpern, J. *Science* **1982**, *217*, 401–407.
- (14) Brown, J. M.; Chaloner, P. A. In *Homogeneous Catalysis with Metal Phosphine Complexes*; Pignolet, L. H., Ed.; Plenum: New York, 1983; p 137.
- (15) Brown, J. M. *Chem. Soc. Rev.* **1993**, *22*, 25–41.
- (16) Boudart, M.; Djegamariadassou, G. *Catal. Lett.* **1994**, *29*, 7–13.
- (17) Heller, D.; Thede, R.; Haberland, D. *J. Mol. Catal. A-Chem.* **1997**, *115*, 273–281.
- (18) Landis, C.; Halpern, J. *J. Am. Chem. Soc.* **1987**, *109*, 1746–1754.
- (19) Sun, Y. K.; Landau, R. N.; Wang, J.; LeBlond, C.; Blackmond, D. G. *J. Am. Chem. Soc.* **1996**, *118*, 1348–1353.
- (20) Bircher, H.; Bender, B. R.; von Phillipsborn, W. *Magn. Reson. Chem.* **1993**, *31*, 293–298.

(21) Chan, A. S. C.; Pluth, J. J.; Halpern, J. *J. Am. Chem. Soc.* **1980**, *102*, 5952–5954.

(22) Brown, J. M.; Chaloner, P. A. *J. Chem. Soc., Chem. Commun.* **1980**, 344–346.

(23) Bosnich, B., Ed. *Asymmetric Catalysis*; Martinus Nijhoff: Dordrecht, 1986; Vol. 103.

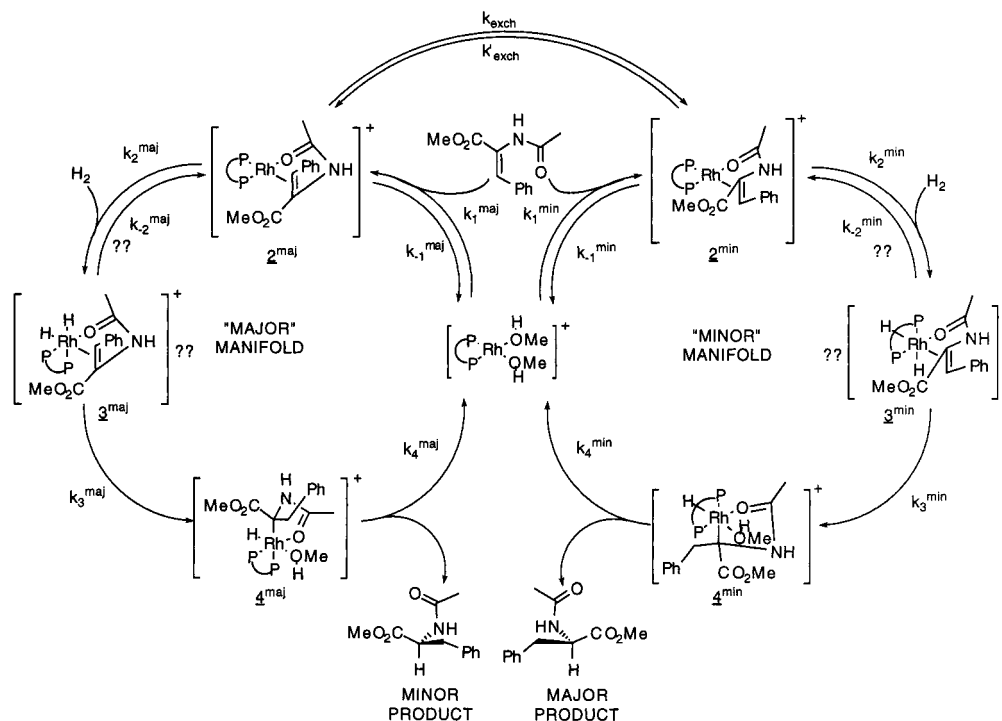


**Figure 1.** General mechanistic scheme for asymmetric hydrogenation. Question marks (??) indicate uncharacterized steps and intermediates.

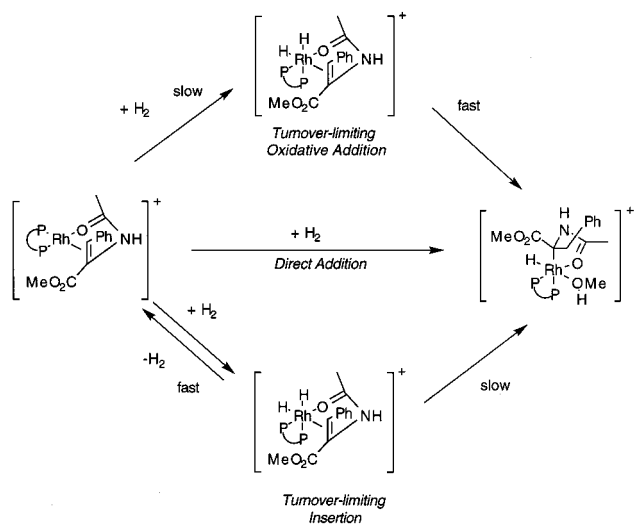


**Figure 2.** Three kinetic schemes that are consistent with the empirical rate data.

the transition-state structure for the step in which the product enantioselectivity is irreversibly fixed, new catalysts may be designed to maximize the enantiodifferentiation.

For the catalytic, enantioselective hydrogenation of prochiral enamides, the exact nature of the turnover-limiting and enantiodetermining step(s) is unclear.<sup>24,25</sup> Kinetic and spectroscopic studies<sup>18</sup> clearly indicate that the turnover-limiting step is enantiodetermining, and, in keeping with the first-order dependence of the rate on H<sub>2</sub> concentration, molecular hydrogen is involved in this step. However, at least three mechanistic pathways (Figure 2) are consistent with existing data:<sup>24</sup> (1) enantiodetermining and *turnover-limiting oxidative addition* of H<sub>2</sub> to the enamide-catalyst adduct, yielding a dihydride

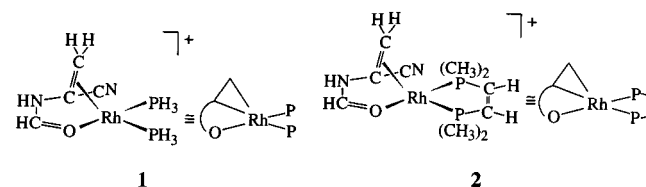


**Figure 3.** Model systems **1** and **2** and their abbreviated graphical representations.

intermediate; (2) *direct addition* of H<sub>2</sub> to the catalyst enamide adduct to form a metal alkyl hydride in a concerted fashion; and (3) reversible, endergonic addition of H<sub>2</sub> to the enamide-catalyst adduct, followed by *turnover-limiting insertion* of the alkene into a metal-hydrogen bond to form a metal alkyl. These distinctions are critical to understanding the origins of enantio-determination in asymmetric hydrogenation because the transition states of the different pathways will have significantly different structures and steric influences. As a first step to resolving these issues, we report the results of DFT computations of the catalytic reaction potential energy surface for a simple, achiral model system.

This paper begins with a description of the model systems studied, the computational models employed, and the rationale for their selection. Next, we describe the overall reaction pathways explored in the computations and summarize key findings. In subsequent sections we discuss essential details of intermediate and transition-state structures. In the penultimate section we present estimations of kinetic isotope effects in enamide hydrogenation and the role of isomerization pathways in the catalytic reaction. We conclude by comparing features of the computationally derived mechanism with relevant empirical data.

## II. Model Systems and Computational Methods

Model complex **1** (Figure 3) was chosen to mimic the structural and electronic features of catalytic systems while minimizing computational time. Model **1**, which corresponds to the enamide-catalyst adducts of Figure 1, consists of a cationic rhodium with two *cis*-ligated

(24) Brauch, T. W.; Landis, C. R. *Inorg. Chim. Acta* **1998**, 270, 285–297.

(25) Giovannetti, J. S.; Kelly, C. M.; Landis, C. R. *J. Am. Chem. Soc.* **1993**, 115, 4040–4057.

phosphines and a coordinated enamide moiety. As found experimentally, the enamide coordinates in a bidentate fashion. In our model we have included an electron-withdrawing nitrile in the  $\alpha$ -position in order to simulate enamide substrates which yield high enantioselectivity in the experimental systems.<sup>26,27</sup> We have performed computations on a larger model system, model 2, also. In 2, the simple  $\text{PH}_3$  ligands have been replaced by the chelating diphosphine, *cis*-1,2-bis(dimethylphosphino)ethane. This model was selected to better model the electronic and geometric features of the highly effective ligand, DuPHOS.<sup>5</sup> All calculations were performed with Gaussian94.<sup>28</sup>

**Geometry Optimizations.** All intermediate and transition-state geometries were optimized using density functional theory (DFT), with Becke's three-parameter functional (B3)<sup>29</sup> and Lee, Yang, and Parr (LYP) correlation energies.<sup>30</sup> The B3LYP method exhibits accuracy comparable to that of sophisticated post-Hartree-Fock methods in other transition metal studies.<sup>31</sup> The double- $\zeta$  quality, Hay and Wadt LANL2DZ basis set for the valence and penultimate shells, with effective core potentials at rhodium<sup>32</sup> and phosphorus,<sup>33</sup> and a Dunning/Huzinaga full double- $\zeta$  basis<sup>34</sup> on C, H, N and O, was used for initial studies. This set of basis functions and effective core potentials is referred to as Basis I throughout this work. In selected cases, geometry optimizations were performed using the more sophisticated basis sets and effective core potentials from the Stuttgart group: these computations used effective core potentials for rhodium<sup>35</sup> and phosphorus,<sup>36</sup> replacing 28 and 10 core electrons, respectively. The valence basis sets from Stuttgart used the following contraction schemes: (311111/22111/411) for rhodium and (31/31) for phosphorus. For phosphorus, one d function with an exponent of 0.34<sup>37</sup> was added. For all other non-hydrogen atoms a 6-31G(d) basis was utilized.<sup>38-42</sup> The hydrogen atom basis set was augmented by a p-type polarization function (6-31G(dp) basis set). This basis set will be referred to as Basis II throughout this work.

No symmetry or internal coordinate constraints were applied. For all intermediates (i.e., true minima) on the potential energy surface (molecular  $\text{H}_2$  complexes, dihydride complexes, alkyl hydride complexes), we attempted to find geometry-optimized minima for all possible geometric isomers starting from multiple initial structures. All reported intermediates are true minima, as determined by the absence of any negative eigenvalue in the vibrational frequency analysis. Transition-state structures (indicated by ‡) were located using the synchronous-guided quasi-Newton method (STQN) until the Hessian

(26) Brown, J. M.; Parker, D. *Organometallics* **1982**, *1*, 950–956.

(27) Koenig, K. E.; Bachman, G. L.; Vineyard, B. D. *J. Org. Chem.* **1980**, *45*, 2362–2365.

(28) Frisch, M. J.; Trucks, G. W.; Schlegel, H. B.; Gill, P. M. W.; Johnson, B. G.; Robb, M. A.; Cheeseman, J. R.; Keith, T.; Petersson, G. A.; Montgomery, J. A.; Raghavachari, K.; Al-Laham, M. A.; Zakrzewski, V. G.; Ortiz, J. V.; Foresman, J. B.; Cioslowski, J.; Stefanov, B. B.; Nanayakkara, A.; Challacombe, M.; Peng, C. Y.; Ayala, P. Y.; Chen, W.; Wong, M. W.; Andres, J. L.; Replogle, E. S.; Gomperts, R.; Martin, R. L.; Fox, D. J.; Binkley, J. S.; Defrees, D. J.; Baker, J.; Stewart, J. P.; Head-Gordon, M.; Gonzalez, C.; Pople, J. A. *Gaussian 94*, Revision D4; Gaussian, Inc.: Pittsburgh, PA, 1995.

(29) Becke, A. D. *Phys. Rev. A* **1988**, *38*, 3098.

(30) Lee, C.; Yang, W.; Parr, R. G. *Phys. Rev. B* **1988**, *37*, 785–789.

(31) Schmid, R.; Herrmann, W. A.; Frenking, G. *Organometallics* **1997**, *16*, 701–708.

(32) Hay, P. J.; Wadt, W. R. *J. Chem. Phys.* **1985**, *82*, 299–310.

(33) Hay, P. J.; Wadt, W. R. *J. Chem. Phys.* **1985**, *82*, 285–298.

(34) Dunning, T. H.; Hay, P. J. In *Modern Theoretical Chemistry*; Schaefer, H. F., III, Ed.; Plenum: New York, 1976; Vol. 3, p 1.

(35) Andrae, D.; Häussermann, U.; Dolg, M.; Stoll, H.; Preuss, H. *Theor. Chim. Acta* **1990**, *77*, 123–142.

(36) Bergner, A.; Dolg, M.; Küchle, W.; Stoll, H.; Preuss, H. *Mol. Phys.* **1993**, *80*, 1431–1441.

(37) Huzinaga, S. *Gaussian Basis Sets for Molecular Calculations*; Elsevier: Amsterdam, 1984.

(38) Ditchfield, R.; Hehre, W. J.; Pople, J. A. *J. Chem. Phys.* **1971**, *54*, 724–728.

(39) Hehre, W. J.; Ditchfield, R.; Pople, J. A. *J. Chem. Phys.* **1972**, *56*, 2257–2261.

(40) Hariharan, P. C.; Pople, J. A. *Theor. Chim. Acta* **1973**, *28*, 213–222.

(41) Hariharan, P. C.; Pople, J. A. *Mol. Phys.* **1974**, *27*, 209–214.

(42) Gordon, M. S. *Chem. Phys. Lett.* **1980**, *76*, 163–171.

**Table 1.** Influences of Basis Set II and Model 1 (Acronyms Described in Text)

| structure                         | optimization  | single-point                      | optimization   |
|-----------------------------------|---------------|-----------------------------------|----------------|
|                                   | model 1       | model 1                           | model 1        |
|                                   | B3LYP/Basis I | B3LYP/Basis II//<br>B3LYP/Basis I | B3LYP/Basis II |
| MOLH <sub>2</sub> -A              | +0.8          | -0.7                              | -1.2           |
| MOLH <sub>2</sub> -A <sup>‡</sup> | +11.1         | +5.5                              | +5.5           |
| DIHY-A                            | +4.9          | +1.3                              | +1.0           |
| DIHY-A <sup>‡</sup>               | +13.2         | +8.6                              | +8.4           |
| DIHY-A→B <sup>‡</sup>             | +14.1         | +11.3                             | +11.7          |
| DIHY-B                            | +1.6          | -2.8                              | -2.3           |
| DIHY-B <sup>‡</sup>               | +2.6          | +7.3                              | -1.4           |
| ALHY-A $\alpha$                   | -19.5         | -20.1                             | -20.5          |

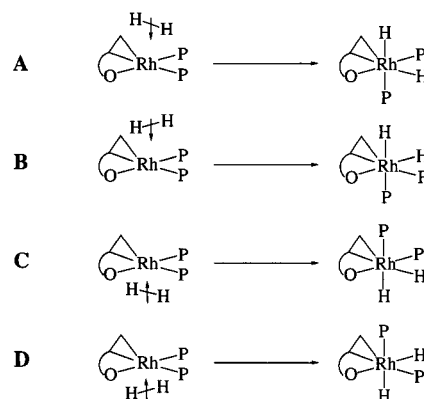


**Figure 4.** Isomers of dihydrides that may be formed from the addition of  $\text{H}_2$  to  $[\text{Rh}(\text{PH}_3)_2(\alpha\text{-formamidoacrylonitrile})]^+$ .

matrix had only one imaginary eigenvalue. For the successful transition-state optimizations of SQPL-C<sup>‡</sup> and SQPL-A<sup>‡</sup> (vide infra), whose potential surfaces are very flat, it was necessary to provide starting structures for the transition-state optimization generated by relaxed potential energy surface scans along a Rh–H distance coordinate. For all transition states of model 1, intrinsic reaction coordinate calculations (IRC) in mass-weighted internal coordinates were performed in both directions.

**Energies.** Our convention for indicating the methods of computing the total energy and performing geometry optimizations are exemplified by the designation “B3LYP/Basis II//B3LYP/Basis I”. This designation represents a geometry optimization performed with Basis I and a total energy computed with Basis II. Single-point calculations of all B3LYP/Basis I-optimized geometries and transition states were performed at the B3LYP/Basis II level. In addition, further optimizations of selected intermediates and transition states were performed at the B3LYP/Basis II level.

The addition of f-polarization functions has been found to be important for the calculation of energies of transition metal complexes in high oxidation states. To test these effects for our model system, we performed B3LYP/Basis II//B3LYP Basis I calculations using an additional f-function with an exponent of 1.35<sup>43</sup> on several intermediates in the catalytic cycle. The calculated energies reveal only small changes (<0.05 kcal/mol) in the relative energies of the intermediates. Therefore, we excluded further use of f-polarization functions in our study.

The changes in relative energies obtained by applying Basis I vs Basis II to structures optimized with Basis I (i.e., B3LYP/Basis II//B3LYP/Basis I vs B3LYP/Basis II//B3LYP/Basis I) follow an overall trend: the relative energies of stable intermediates and transition-state energies are reduced by 0–4 and 2–6 kcal/mol, respectively, for Basis II energies relative to Basis I energies. In some cases larger deviations were found. For such cases, we reoptimized the geometry at the B3LYP/Basis II level. In addition, the structures which are proposed to be important in the energetically favored reaction pathway A (vide infra)

(43) Ehlers, A. W.; Böhme, M.; Dapprich, S.; Gobbi, A.; Höllwarth, A.; Jonas, V.; Köhler, K. F.; Stegman, R.; Veldkamp, A.; Frenking, G. *Chem. Phys. Lett.* **1993**, *208*, 111–114.

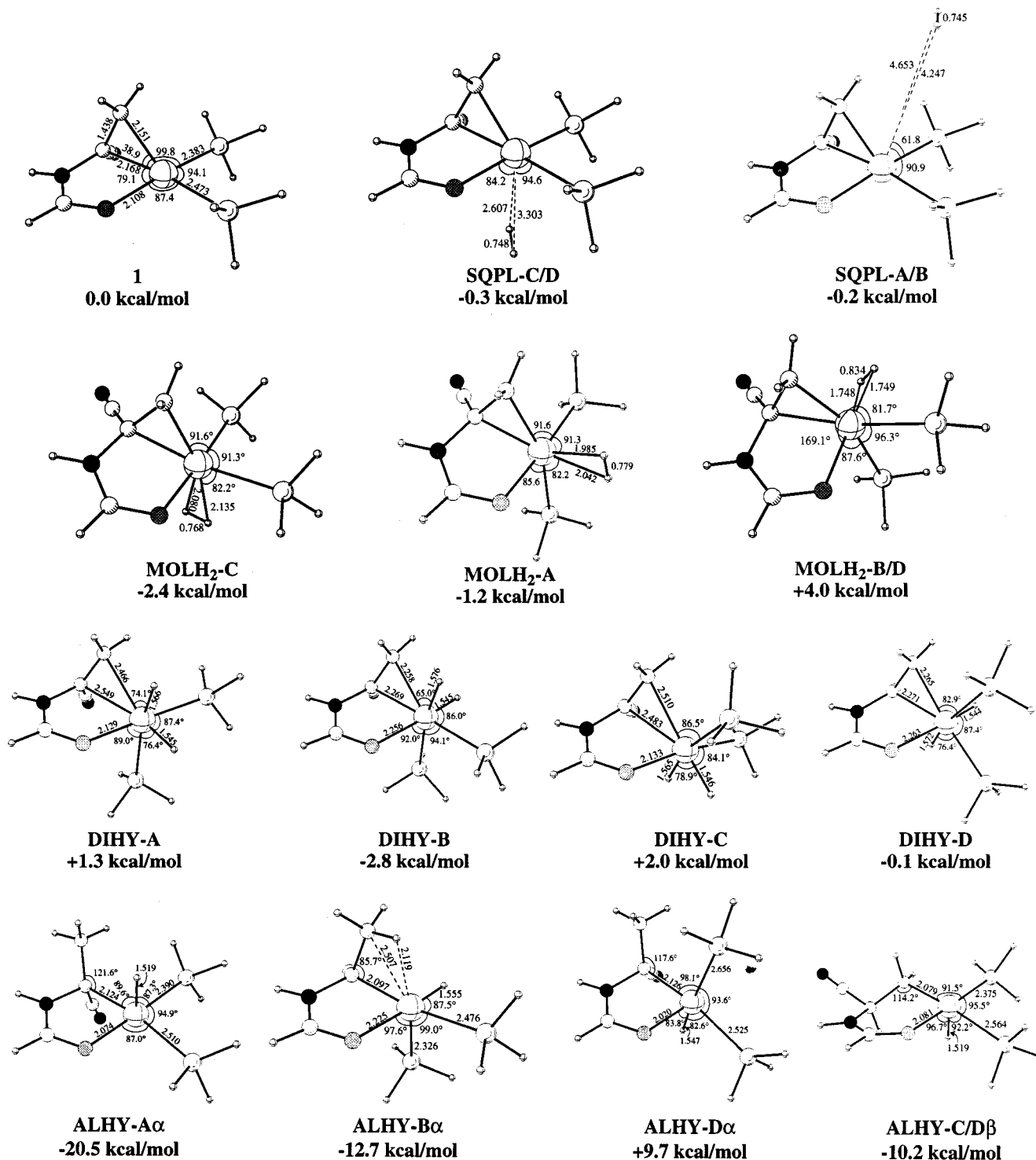


**Figure 5.** Geometry-optimized structures of intermediates that lie along the primary reaction pathways.

were reoptimized as well. For these structures, the changes in relative energies were smaller than 0.4 kcal/mol. The relative energies for the reoptimized structures are used in Figure 7 and for discussion. Table 1 summarizes B3LYP/Basis I//B3LYP/Basis I energies and B3LYP/Basis II//B3LYP/Basis I energies for model system **1**.

### III. Computational Results

**The Nature of the H<sub>2</sub> Activation Step: Concerted or Stepwise?** Our first concern is distinguishing among the modes of H<sub>2</sub> activation outlined in Figure 2. The “direct addition” mode is unique in that it does not involve a dihydride intermediate; rather, this path describes concerted addition of H<sub>2</sub> to **1** to yield

an alkyl hydride via passage over a single activation barrier. Despite extensive computational searching, and despite finding (vide infra) stable dihydrogen complexes and alkyl hydrides that might serve as the reactants and products, respectively, for a concerted pathway, we were unable to find any evidence for this pathway. Instead, we have found extensive computational support for the intermediacy of dihydrides in the catalytic reaction.

**Overview of the Reaction Mechanism.** Overall, we have found that catalytic hydrogenation follows the sequence: cationic alkene complex (**1**)  $\rightarrow$  ion-induced dipole complex of

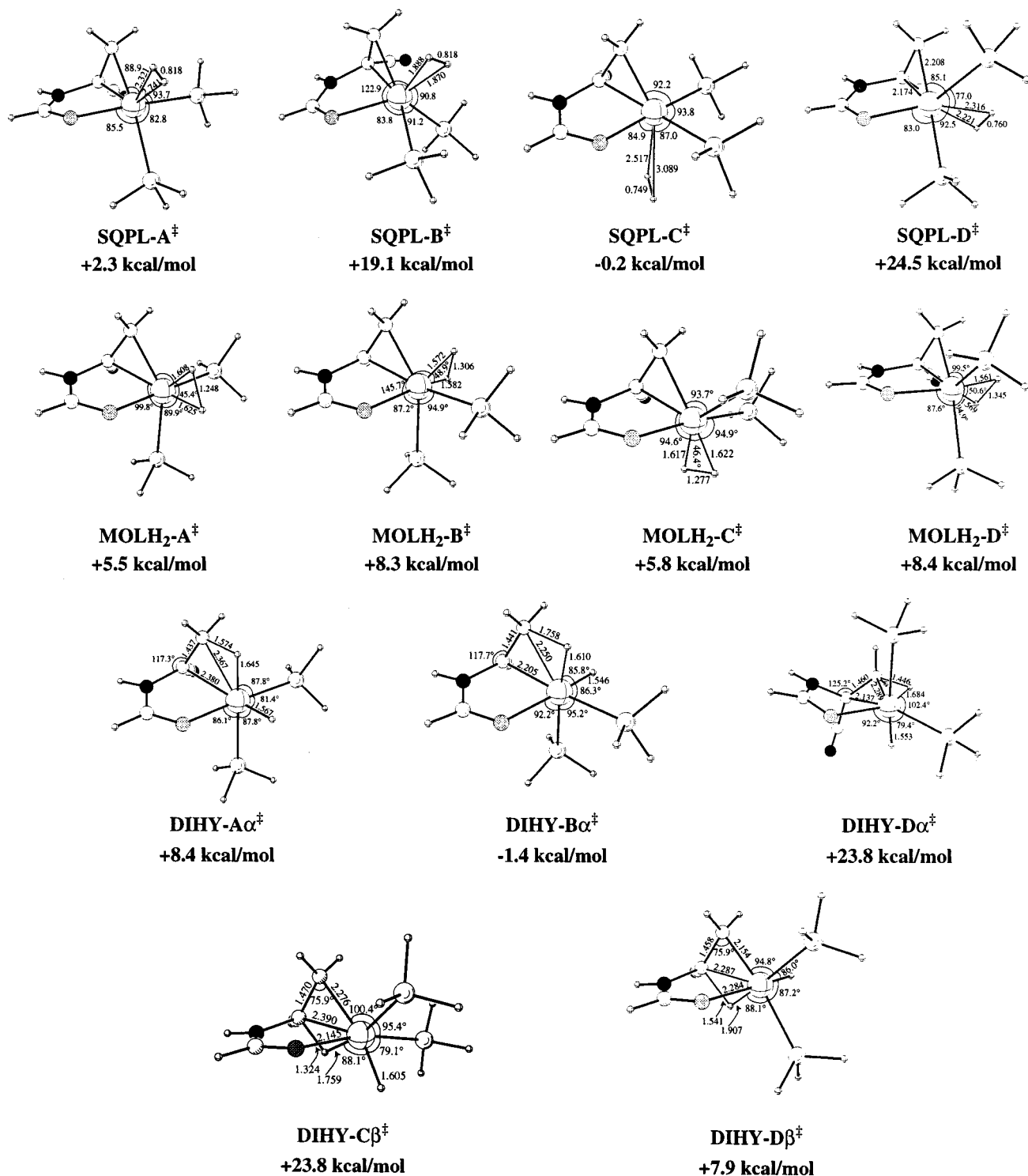


**Figure 6.** Structures of transition states found along the primary reaction pathways.

H<sub>2</sub> with the square planar alkene complex (SQPL) → molecular H<sub>2</sub> complex (MOLH<sub>2</sub>) → dihydride complex (DIHY) → alkyl hydride complex (ALHY) → coordinated alkane product (PROD). The exploration of the catalytic cycle is complicated by the presence of multiple isomeric pathways. In principle, oxidative addition of H<sub>2</sub> to a chelated, square planar complex can form four different dihydrides with cis configurations,<sup>44,45</sup> as shown in Figure 4. Thus, a minimum of four pathways must

be considered in the modeling; these pathways are differentiated by A, B, C, or D in the structure labels (e.g., DIHY-A and MOLH<sub>2</sub>-C).

Further divergence of pathways occurs at the alkyl hydride stage because either  $\alpha$ - or  $\beta$ -alkyl hydrides may be formed. These isomers are indicated by  $\alpha$  and  $\beta$  in the structural labels (e.g., ALHY-A $\alpha$ , indicating the  $\alpha$ -alkyl hydride complex formed from the dihydride, DIHY-A).

In Figures 5 and 6, we present the optimized structures along the primary reaction pathways. A reaction coordinate diagram that illustrates the primary reaction pathways is shown in Figure

(44) Brown, J. M.; Evans, P. L. *Tetrahedron* **1988**, *44*, 4905–4916.

(45) Bogdan, P. L.; Irwin, J. J.; Bosnich, B. *Organometallics* **1989**, *8*, 1450–1453.

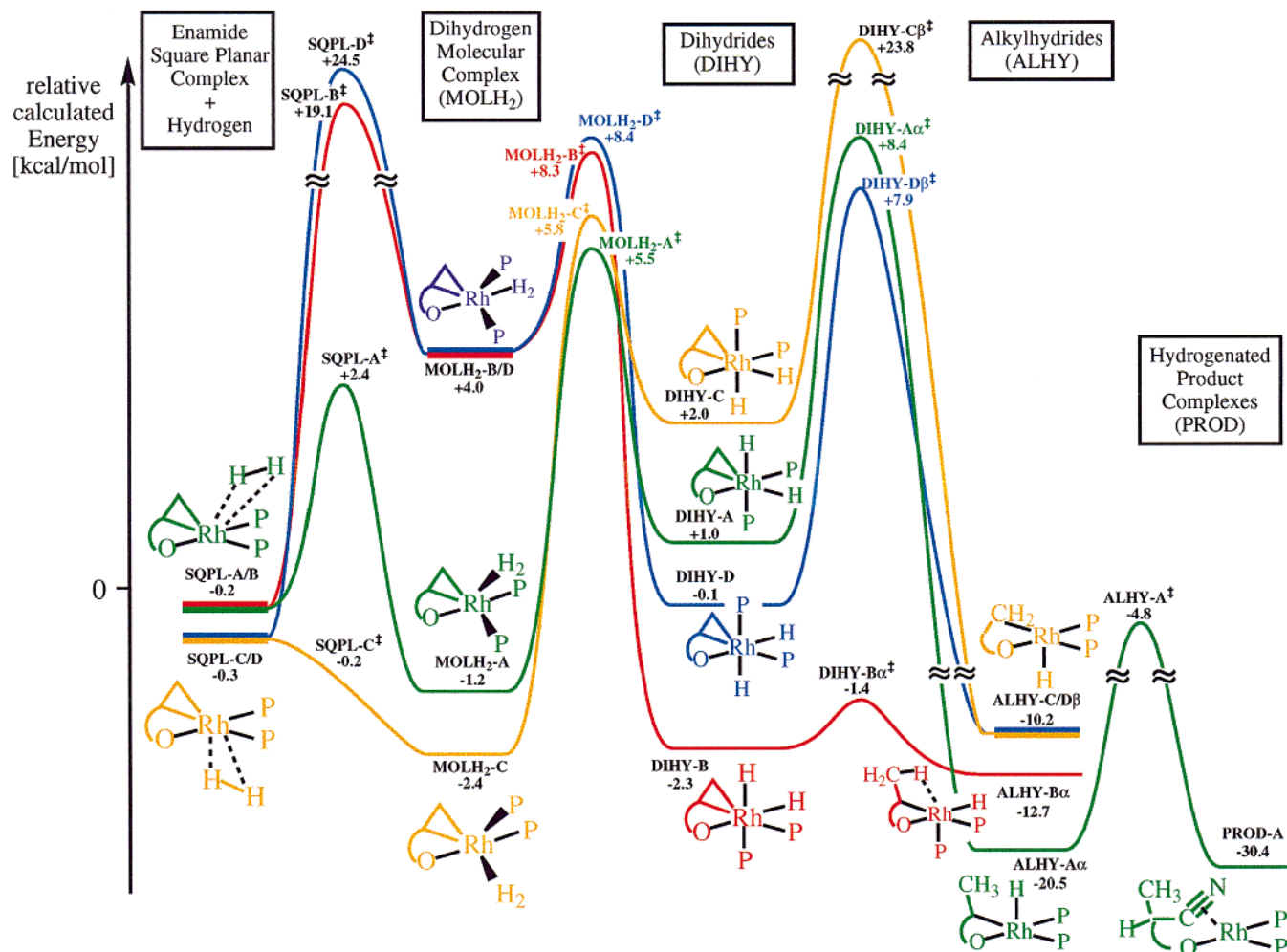


**Figure 7.** Potential energy surface for the reaction of model **1** with H<sub>2</sub>.

**Table 2.** Structural Features of [Rhodium(enamide)(diphosphine)]<sup>+</sup> Complexes and Ion-Induced Dipole Complexes with H<sub>2</sub>

|                                     | X-tal 1 <sup>a</sup> | X-tal 2 <sup>b</sup> | X-tal 3 <sup>c</sup> | 1 <sup>d</sup> (Basis I) | 1 <sup>d</sup> (Basis II) | 2     | SQPL-A/B | SQPL-C/D |
|-------------------------------------|----------------------|----------------------|----------------------|--------------------------|---------------------------|-------|----------|----------|
| Bonds (Å)                           |                      |                      |                      |                          |                           |       |          |          |
| Rh–O                                | 2.113(5)             | 2.128(5)             | 2.108(13)            | 2.108                    | 2.128                     | 2.141 | 2.111    | 2.107    |
| Rh–C <sub>α</sub>                   | 2.195(8)             | 2.171(8)             | 1.995(24)            | 2.168                    | 2.160                     | 2.184 | 2.168    | 2.166    |
| Rh–C <sub>β</sub>                   | 2.246(6)             | 2.197(8)             | 2.049(18)            | 2.151                    | 2.144                     | 2.141 | 2.151    | 2.140    |
| Rh–P <sub>trans</sub> O             | 2.228(2)             | 2.232(2)             | 2.239(6)             | 2.383                    | 2.293                     | 2.371 | 2.382    | 2.384    |
| Rh–P <sub>trans</sub> C             | 2.271(2)             | 2.289(2)             | 2.272(6)             | 2.473                    | 2.393                     | 2.430 | 2.472    | 2.474    |
| C <sub>α</sub> –C <sub>β</sub>      | 1.382(12)            |                      | 1.227(24)            | 1.438                    | 1.414                     | 1.438 | 1.437    | 1.443    |
| Angles (deg)                        |                      |                      |                      |                          |                           |       |          |          |
| O–Rh–C <sub>α</sub>                 | 77.8(2)              | 78.0(3)              | 77.8(7)              | 79.1                     | 78.8                      | 78.5  | 79.0     | 79.0     |
| C <sub>α</sub> –Rh–P <sub>cis</sub> | 109.6(2)             | 109.0(2)             | 107.5(6)             | 99.8                     | 100.0                     | 103.1 | 99.7     | 99.8     |
| P–Rh–P                              | 83.0(1)              | 83.1(1)              | 83.1(2)              | 94.1                     | 92.9                      | 84.4  | 94.1     | 93.9     |
| O–Rh–P <sub>cis</sub>               | 88.9(2)              | 89.8(2)              | 92.6(4)              | 87.4                     | 88.7                      | 94.4  | 87.5     | 88.1     |
| C <sub>α</sub> –Rh–C <sub>β</sub>   | 36.2(3)              | 36.9(4)              |                      | 38.9                     | 38.7                      | 38.8  | 38.3     | 39.2     |

<sup>a</sup> [Rh(DIPHOS)(methyl-(Z)-α-acetamidocinnamate)](BF<sub>4</sub>).<sup>46</sup> <sup>b</sup> [Rh(S,S-CHIRAPHOS)(ethyl-(Z)-α-acetamidocinnamate)](ClO<sub>4</sub>).<sup>46</sup> <sup>c</sup> [Rh(R,R-DIPAMP)(methyl-(Z)-β-propyl-α-acetamidoacrylate)](BF<sub>4</sub>).<sup>47</sup> <sup>d</sup> Optimized with the basis set given in parentheses.

7. We now trace the computational reaction pathway, starting with the square planar alkene complex **1** and following its reaction with H<sub>2</sub> to yield alkane product.

**Structures of Rh Alkene and Ion-Induced Dipole Complexes.** Three [Rh(enamide)(diphosphine)]<sup>+</sup> crystal structures have been published over the last 18 years: [Rh(DIPHOS)(methyl-(Z)-α-acetamidocinnamate)](BF<sub>4</sub>),<sup>46</sup> [Rh(S,S-CHIRAPHOS)(ethyl-(Z)-α-acetamidocinnamate)](ClO<sub>4</sub>),<sup>21</sup> and [Rh(R,R-DIPAMP)(methyl-(Z)-β-propyl-α-acetamidoacrylate)](BF<sub>4</sub>).<sup>47</sup>

(CHIRAPHOS = 2,3-bis(diphenylphosphino)butane; DIPAMP = 1,2-bis(phenyl-*o*-anisylphosphino)ethane). The DIPAMP structure is the least well characterized of the three and contains an unusually short coordinated olefin bond with a large estimated deviation, 1.227(24) Å. Therefore, the structural data of this study should be considered with caution. Structural data for computational model complexes (**1**, **2**, and the ion-induced dipole structures SQPL-A/B and SQPL-C/D) are collected alongside empirical structural data in Table 2. The calculated

(46) Chan, A. S. C.; Pluth, J. J.; Halpern, J. *Inorg. Chim. Acta* **1979**, *37*, L477–L479.

(47) McCullough, B.; Halpern, J.; Thompson, M. R.; Landis, C. R. *Organometallics* **1990**, *9*, 1392–1395.

bond lengths and angles show reasonable agreement with experimental data. The expected trans influence, yielding a longer Rh–P bond trans to the coordinated olefin than trans to the coordinated amide carbonyl, is well reproduced. The significantly shorter rhodium–phosphorus bonds in the crystal structures probably reflect both the deficiencies of the basis sets employed (Basis II yields a Rh–P bond length that is shorter than that of Basis I by 0.08 Å) and intrinsic differences between aryl phosphines and phosphines bonded to H or alkyl groups. Our results are consistent with previous computations by Selke and co-workers.<sup>48</sup>

Addition of H<sub>2</sub> to **1** to form ion–induced dipole complexes, **SQPL-A/B** and **SQPL-C/D**, does not perturb the structural parameters of alkene complexes significantly. The primary difference between the two ion–induced dipole complexes is the Rh–H<sub>2</sub> distance. In **SQPL-A/B**, which has steric repulsion between the enamide methylene and the coordinated H<sub>2</sub>, the H<sub>2</sub>–Rh distance is 1.5 Å longer than that in **SQPL-C/D**. Formation of the ion–dipole complexes is slightly exothermic according to B3LYP (ca. –0.2 kcal/mol).

**Conversion of Ion–Induced Dipole Complexes into Molecular H<sub>2</sub> Complexes.** Three dihydrogen complexes (**MOLH<sub>2</sub>-A**, **MOLH<sub>2</sub>-B/D**, and **MOLH<sub>2</sub>-C**) were found to be stable intermediates within the catalytic cycle. In the nomenclature adopted here, the A, B/D, and C labels indicate which rhodium dihydride isomer(s) are formed from each of the dihydrogen complexes. All three dihydrogen complexes exhibit nearly ideal trigonal bipyramidal geometry, with the amido oxygen in an axial position. We note that all structures with trans phosphine arrangements were excluded from consideration because our interest is in modeling chelating diphosphine catalysts. Thus, the strong preference of the donor oxygen atom for the axial position, a feature that is mirrored in main group trigonal bipyramidal structures, dominates the structures of the dihydrogen complexes. Rationalization of the observed site preferences follows arguments developed by Hoffmann:<sup>49</sup> in five-coordinate d<sup>8</sup> transition metal complexes, the stronger  $\sigma$ -donor ligand prefers the axial position and the  $\pi$ -acceptor ligand the equatorial position. Morokuma<sup>50</sup> has found similar site preferences in computations for RhH(C<sub>2</sub>H<sub>4</sub>)(CO)<sub>2</sub>(PH<sub>3</sub>). Although the dihydrogen complexes vary in energy (–2.4, –1.2, and 4.0 kcal/mol for isomers C, A, and B/D, respectively), all isomers are viable catalytic intermediates on thermodynamic grounds.

However, not all dihydrogen complex isomers are kinetically accessible. Approach of dihydrogen from either face of the initial square planar geometry may occur with a low energy barrier when the H–H vector is approximately parallel with the Rh–alkene bond. These approaches yield **MOLH<sub>2</sub>-A** and **MOLH<sub>2</sub>-C** via the transition states **SQPL-A<sup>‡</sup>** (+2.4 kcal/mol) and **SQPL-C<sup>‡</sup>** (–0.2 kcal/mol), respectively. In marked contrast, approaches of dihydrogen from either face of the square plane with the H–H bond parallel to the Rh–O bond (**SQPL-B<sup>‡</sup>** and **SQPL-D<sup>‡</sup>**) have high barriers (19.1 and 24.5 kcal/mol) and lead to the same dihydrogen complex, **MOLH<sub>2</sub>-B/D**. Thus, only the dihydrogen complexes **MOLH<sub>2</sub>-A** and **MOLH<sub>2</sub>-C** are accessible on kinetic grounds.

We rationalize the high barriers for the formation of **MOLH<sub>2</sub>-B/D** from a least motion perspective.<sup>51</sup> In order for **1** to

transform into the trigonal bipyramidal structure of **MOLH<sub>2</sub>-B/D** with a trans disposition of the amido oxygen and dihydrogen, both phosphine ligands must move out of the coordination plane of the original square planar complex. Similarly, H<sub>2</sub> must initially approach the square plane from a perpendicular direction but then migrate into the original coordination plane. Thus, formation of the **SQPL-B<sup>‡</sup>** and **SQPL-D<sup>‡</sup>** transition states involves extensive nuclear and electronic reorganization and, hence, large barriers.

*Dihydrogen complexes are not only sufficient, but appear to be necessary, intermediates for the formation of rhodium dihydrides in our model systems.* All attempts to find transition states that convert **1** into the dihydrides **DIHY-A**, **-B**, **-C**, or **-D** converged on the transition states either for formation of molecular hydrogen complexes or for the conversion of dihydrogen complexes into dihydrides. Similarly, relaxed scans of the potential energy surface along the two Rh–H distance coordinates failed to reveal alternate low-energy paths for forming dihydrides.

**Conversion of Dihydrogen Complexes to Metal Dihydrides.** We have found that all four dihydride complexes (**DIHY-A**, **-B**, **-C**, and **-D**) that can result from cis oxidative addition of H<sub>2</sub> to **1** are thermodynamically accessible minima on the reaction potential energy surface. Formation of dihydrides from **1** and H<sub>2</sub> is approximately thermoneutral; reaction enthalpies range from –2.3 to +2.0 kcal/mol. If one assumes a 10 kcal/mol entropic contribution to the free energy of reaction of **1** and H<sub>2</sub> to form dihydrides at these temperatures, then the computed reaction free energies vary from +7.7 to 12 kcal/mol. These free energies are endergonic enough that the equilibrium concentrations of the dihydride intermediates are expected to be very low even under high pressures of dihydrogen. *Although all dihydrides are thermodynamically accessible, only DIHY-A and DIHY-C are kinetically accessible* (disregarding, for now, any isomerization pathways) due to the high barriers to formation of the molecular hydrogen precursor (**MOLH<sub>2</sub>-B/D**) for **DIHY-B** and **DIHY-D**.

Each of the dihydrides has one hydrogen trans to a phosphine. The lower energy dihydrides (**DIHY-B** and **-D**) place the remaining hydrogen trans to the oxygen whereas the higher energy dihydrides (**DIHY-A** and **-C**) have that hydrogen trans to the C=C double bond. The relative energies of the dihydride isomers may be considered the result of slight differences in trans influences: the most stable arrangement is for the most electronegative ligand to be placed trans to the hydride ligand.<sup>52</sup>

*Procession from the dihydrogen complexes to the four dihydride intermediates (DIHY-A, -B, -C, -D) occurs with low barriers ranging from 4.3 to 8.2 kcal/mol.* Thus, once the dihydrogen complexes are reached, they easily proceed to the corresponding dihydrides. The geometries of these transition states have significantly longer H–H distances (ranging from 1.248 to 1.345 Å) than the molecular hydrogen complexes (0.768–0.834 Å), indicating that the barrier corresponds primarily to stretching the H–H bond. The structures of the transition states do not follow the Hammond postulate.<sup>53</sup> The two transition states for exothermic formation of dihydrides (**MOLH<sub>2</sub>-D<sup>‡</sup>** and **MOLH<sub>2</sub>-B<sup>‡</sup>**) involve changes in the H–H distances (0.511 and 0.472 Å, respectively) similar to those of the transition states for endothermic dihydride formation (**MOLH<sub>2</sub>-C<sup>‡</sup>**, 0.509 Å; **MOLH<sub>2</sub>-A<sup>‡</sup>**, 0.469 Å).

**Conversion of Dihydrides into Alkyl Hydrides.** Migratory insertion of a C=C bond into a Rh–H bond of a dihydride

(48) Kless, A.; Borner, A.; Heller, D.; Selke, R. *Organometallics* **1997**, *16*, 2096–2100.

(49) Rossi, A. R.; Hoffmann, R. *Inorg. Chem.* **1975**, *14*, 365–374.

(50) Koga, N.; Jin, S. Q.; Morokuma, K. *J. Am. Chem. Soc.* **1988**, *110*, 3417–3425.

(51) Lowry, T. H.; Richardson, K. S. *Mechanism and Theory in Organic Chemistry*, 2nd ed.; Harper & Row: New York, 1981.

(52) Sargent, A. L.; Hall, M. B.; Guest, M. F. *J. Am. Chem. Soc.* **1992**, *114*, 517–522.

(53) Hammond, G. S. *J. Am. Chem. Soc.* **1955**, *77*, 334–338.

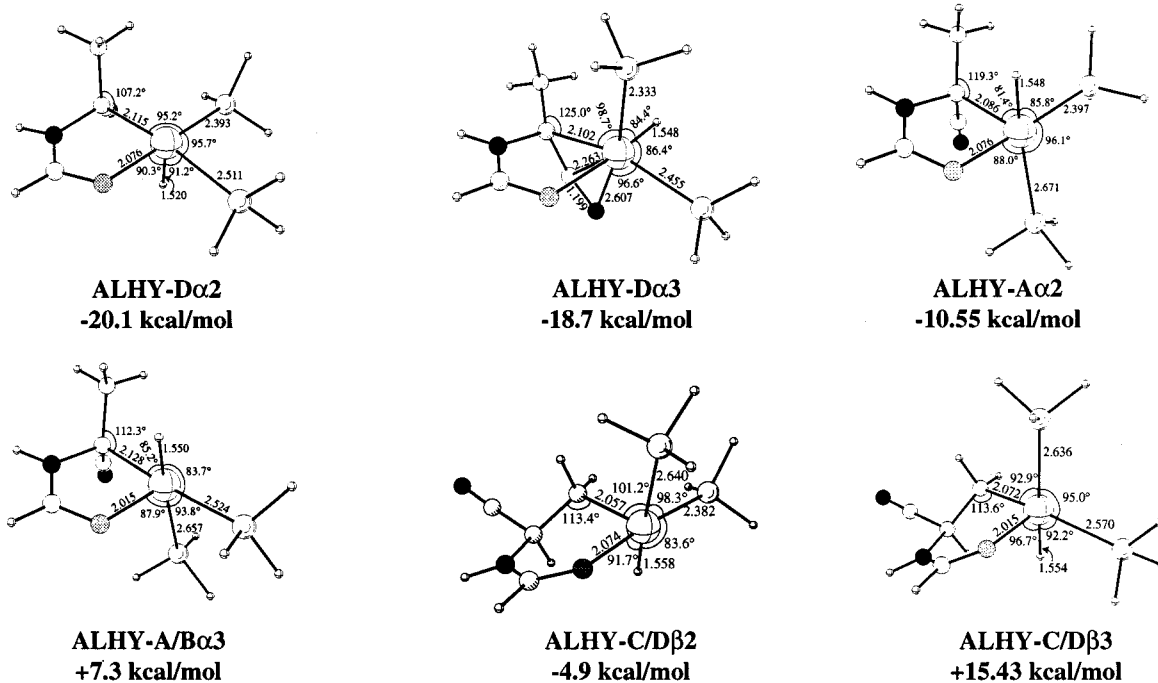


**Figure 8.** Alkyl hydrides that are not direct products of migratory insertion reactions of dihydride intermediates.

intermediate can yield a variety of alkyl hydrides. As the data in Figures 5 and 6 demonstrate, the potential energy surfaces for the conversion of dihydrides into alkyl hydrides span a wide range of enthalpies and activation enthalpies. Although we have searched for all possible alkyl hydride stereoisomers, we have found just seven  $\alpha$ -alkyl hydrides and three  $\beta$ -alkyl hydrides that correspond to true minima on the reaction surface. Alkyl hydride nomenclature, e.g., **ALHY-A $\alpha$** , indicates both the dihydride precursor (A) and the regioisomer ( $\alpha$ ). Four alkyl hydrides result directly from dihydrides (**ALHY-A $\alpha$** , **ALHY-B $\alpha$** , **ALHY-D $\alpha$** , and **ALHY-C/D $\beta$** , see Figure 5). Six alkyl hydrides arise from isomerization (**ALHY-A $\alpha$ 2**, **ALHY-A/ $\beta$  $\alpha$ 3**, **ALHY-D $\alpha$ 2**, **ALHY-D $\alpha$ 3**, **ALHY-C/D $\beta$ 2**, and **ALHY-C/D $\beta$ 3**, see Figure 8) of the direct products of migratory insertion.

All of the alkyl hydrides have an approximate monovalent octahedral structure. The formation of alkyl hydrides from dihydrides may occur via either C=C migration or hydride migration. Both modes are observed computationally. The  $\alpha$ -alkyl hydrides **ALHY-B $\alpha$**  and **ALHY-D $\alpha$**  result from hydride migration, and **ALHY-A $\alpha$**  is the product of C=C migration. The  $\beta$ -alkyl hydride **ALHY-C/D $\beta$**  can result either from **DIHY-C** or **DIHY-D**. Formation of **ALHY-C/D $\beta$**  from **DIHY-C** is the result of C=C migration. In contrast, **DIHY-D** yields **ALHY-C/D $\beta$**  via hydride migration and a rather complex reaction trajectory. The transition states for the direct formation of alkyl hydrides are shown in Figure 6.

A priori, one expects that dihydride intermediates with cis, coplanar orientations of the coordinated C=C bond and Rh-H bond will insert faster than isomers lacking this arrangement. Based on least motion pathways, the dihydrides **DIHY-C** and **DIHY-D** should generate  $\beta$ -alkyl hydrides, and the dihydrides **DIHY-A** and **DIHY-B** should generate  $\alpha$ -alkyl hydrides. These stereochemical kinetic influences are also well supported by the calculated activation energies. The three low barrier insertions, corresponding to transition states **DIHY-B $\alpha$  $^\ddagger$** , **DIHY-A $\alpha$  $^\ddagger$** , and **DIHY-D $\beta$  $^\ddagger$** , each proceed from dihydrides with cis, coplanar orientations and have activation energies relative to the corresponding dihydride reactants of 0.9, 7.4, and 8.0 kcal/mol, respectively. The transition state **DIHY-C $\beta$  $^\ddagger$**  has a high energy

because the initially formed product has mutually trans Rh-H and Rh-C bonds. This initial product is not a true minimum and spontaneously isomerizes to **ALHY-C $\beta$** . In contrast, the high energy of transition state **DIHY-D $\alpha$  $^\ddagger$**  originates in the near orthogonal alignment of the Rh-H vector with respect to the plane of the C=C carbon atoms and Rh in the **DIHY-D** intermediate.

The thermodynamics of alkyl hydride formation are influenced by both the regioselectivity of the insertion reaction (to yield either  $\alpha$ - or  $\beta$ -alkyl hydrides) and the stereochemistry of the alkyl hydride. None of the stable intermediates have geometries with trans Rh-C and Rh-H bonds. All attempts to minimize such structures lead to spontaneous site isomerization, illustrating a powerful trans avoidance of the H ligand. Formation of the three alkyl hydrides (**ALHY-D $\alpha$** , **-A/ $\beta$  $\alpha$ 3**, and **-C/D $\beta$ 2**) from **1** and H<sub>2</sub> is endothermic. In each of these structures, the site trans to the coordinated enamide O is vacant, and the site trans to the H ligand is occupied. For the exothermically formed alkyl hydrides, the position trans to the coordinated enamide O is filled. The most stable  $\alpha$ -alkyl hydrides (**ALHY-A $\alpha$**  and **ALHY-D $\alpha$ 2**) have the hydride in the axial position. Examination of the lone  $\beta$ -isomer (**ALHY-C/D $\beta$** ) that has a hydride in the axial position leads to the conclusion that  *$\beta$ -alkyl hydride formation is intrinsically disfavored by 10 kcal/mol relative to  $\alpha$ -alkyl hydride formation*. Alkyl hydride isomers in which the Rh-C bond is axial (**ALHY-A $\alpha$ 2** and **ALHY-C/D $\beta$ 2**) and isomers which exhibit six-coordination via either a side-bound CN (**ALHY-D $\alpha$ 3**) or a C-H agostic interaction (**ALHY-B $\alpha$** ) also form exothermically from **1** and H<sub>2</sub>. Overall, these energetics are consistent with the expectations of (1) strong trans influences of hydride and alkyl ligands and (2) the stabilization of Rh-C bonds by electron-withdrawing groups, leading to stronger Rh-C( $\alpha$ ) vs Rh-C( $\beta$ ) bonds.

**Alkyl Hydride Reductive Elimination.** Completion of the model catalytic cycle requires computation of the product-forming step. Because this step is not the turnover- and/or selectivity-determining process in catalytic hydrogenation under normal conditions, we have chosen to examine just one reductive elimination pathway. The alkyl hydride **ALHY-A $\alpha$**  smoothly



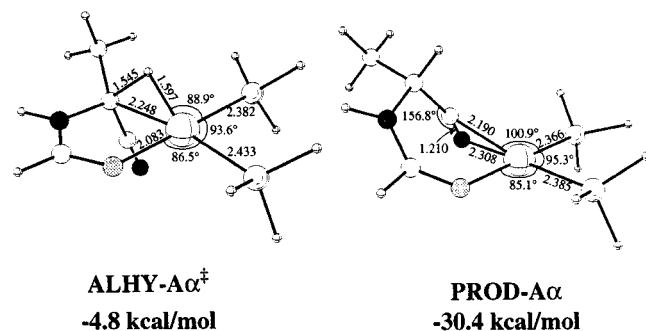


**Figure 9.** Transition state (**ALHY-Aα<sup>‡</sup>**) and product (**PROD-Aα**) structures along the **ALHY-Aα** reductive elimination pathway.

transforms into the hydrogenated product **PROD-Aα** via the transition state **ALHY-Aα<sup>‡</sup>** (see Figure 9). Relative to the alkyl hydride reactant, the reductive elimination barrier is 15.7 kcal/mol, and the reaction is exothermic by 9.9 kcal/mol. The reaction proceeds via net H migration to yield a square planar complex in which both the nitrile and carbonyl of the hydrogenated enamide coordinate to the metal.

**Overview of the Computational Results (Part 1).** The results which have been described thus far are summarized by the reaction coordinate diagram of Figure 7. This reaction coordinate diagram plots total energy, rather than free energy, changes along the reaction pathway. Approximately, this plot maps out enthalpy changes along the reaction pathway. The most significant entropy contribution to the reaction coordinate diagram is the bimolecular association of **H<sub>2</sub>** and **1**. Assuming a value of approximately 10 kcal/mol for this association, the diagram can be converted to free energy terms by lowering the energies of the reactants, **H<sub>2</sub>** + **1**, by 10 kcal/mol.

The primary features of the reaction pathways illustrated in Figure 7 are the following: (1) although formation of the intermediate molecular hydrogen complex **MOLH<sub>2</sub>-B/D** is only mildly endothermic, the very high barrier to formation of **MOLH<sub>2</sub>-B/D** precludes any significant contribution to the reaction rate from simple movement along pathway B or D; (2) simple movement along pathway C, also, cannot make a significant contribution to catalysis because migratory insertion of the dihydride intermediate **DIHY-C** has a very high barrier; (3) simple movement along pathway A does not encounter any large kinetic barriers; and (4) the migratory insertion of **DIHY-A** has a larger barrier than that for reductive elimination of **H<sub>2</sub>** from A to yield the molecular hydrogen complex **MOLH<sub>2</sub>-A**. This result suggests that the reaction pathway should be described as a rapid, endergonic preequilibrium between **1** and **H<sub>2</sub>** to form **DIHY-A**, followed by rate-determining migratory insertion of **DIHY-A** to yield **ALHY-Aα**.

The catalytic cycle is not necessarily as simple as implied by the previous paragraph. The catalytic reaction is not required to stay on a single pathway if there are low-energy isomerization pathways that interconnect different pathways and obviate some of the high barriers. Therefore, we next turn to an examination of isomerization pathways in catalytic enamide hydrogenation.

**Isomerization of Molecular Hydrogen Complexes.** Five-coordinate complexes may undergo site isomerizations with low barriers. Two mechanisms for these site isomerizations are Berry pseudorotation<sup>54</sup> and turnstile rotation. We focus initially on interconversions between the kinetically and thermodynamically favored isomers **MOLH<sub>2</sub>-A** and **MOLH<sub>2</sub>-C** and the higher energy isomer **MOLH<sub>2</sub>-B/D**. In principle, a turnstile rotation could provide a one-step isomerization pathway among the

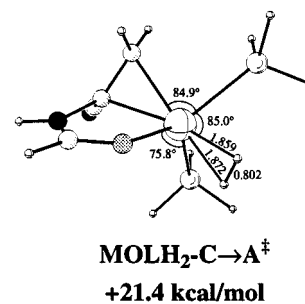


**Figure 10.** Turnstile twist transition-state structure.

isomers. Exhaustive transition-state searches located only one turnstile rotation pathway; this pathway leads from **MOLH<sub>2</sub>-A** to **MOLH<sub>2</sub>-C** via the transition state **MOLH<sub>2</sub>-C → A<sup>‡</sup>** (Figure 10). Due to its high activation energy (ca. 20 kcal/mol) and the similar reactivities of the **MOLH<sub>2</sub>-A** and **MOLH<sub>2</sub>-C** isomers, the turnstile twist rearrangement does not contribute significantly to the catalytic reaction.

A double Berry pseudorotation should, in principle, allow isomerization among the isomers **MOLH<sub>2</sub>-A**, **MOLH<sub>2</sub>-C**, and **MOLH<sub>2</sub>-B/D** (Figure 11). Morokuma<sup>50</sup> has performed computations on related rearrangement pathways for **RhH(C<sub>2</sub>H<sub>4</sub>)(CO)<sub>2</sub>(PH<sub>3</sub>)** and located the transition states for these double Berry pseudorotation isomerizations. Starting from the kinetically unfavored structure **MOLH<sub>2</sub>-B/D**, the first Berry pseudorotation yields a trigonal bipyramidal structure. This intermediate, which has P and C=C in the axial positions, is high in energy (> 15 kcal/mol relative to **MOLH<sub>2</sub>-B/D**). The primary destabilizing influence in this isomer appears to be the placement of the O donor ligand in the equatorial position.

A second Berry pseudorotation leads to the kinetically and thermodynamically favored dihydrogen complexes **MOLH<sub>2</sub>-A** and **MOLH<sub>2</sub>-C**. On the basis of the high energy resulting from the first Berry pseudorotation, the double Berry pseudorotation mechanism is excluded from further consideration.

**Isomerization of Dihydrides.** We searched for two types of pathways connecting the various dihydride intermediates: Bailar twist<sup>55</sup> and ligand dissociative pathways. The Bailar twist mechanism involves rotation of two trigonal faces of the octahedral dihydride complex without breaking any metal–ligand bonds. We could not locate a transition state corresponding to the Bailar twist mechanism; all attempts to locate Bailar twist transition states resulted in alkene dissociation.

Dissociation of the coordinated C=C double bond provides entry to a dihydride isomerization pathway. Because the dihydride **DIHY-B** exhibits a very low migratory insertion barrier but is kinetically inaccessible, we focus on the isomerization pathway that connects the kinetically accessible dihydride **DIHY-A** with the highly reactive intermediate **DIHY-B**. Conversion of **DIHY-A** to **DIHY-B** occurs in three steps (see Figures 12 and 13): (1) decoordination of the C=C ligand and rotation of the H–Rh–H group by 90° relative to the rest of the coordination framework; (2) translation of the O–Rh bond to the adjacent vacant coordination site; and (3) recoordination of the enamide C=C. An overall barrier from **DIHY-A** to **DIHY-B** of 13.1 kcal/mol was determined. This barrier is higher than the barrier for conversion of **DIHY-A** into **ALHY-A**, but only by 2.0 kcal/mol. As a result, it is possible that some of the catalytic hydrogenation flux could proceed along the dihydride isomerization pathway.

**Isotope Effects in Catalytic Hydrogenation.** Kinetic isotope effect measurements provide valuable information concerning

(54) Berry, R. S. *J. Chem. Phys.* **1960**, *32*, 933–938.

(55) Bailar, J. C. *J. Inorg. Nucl. Chem.* **1958**, *8*, 165–175.

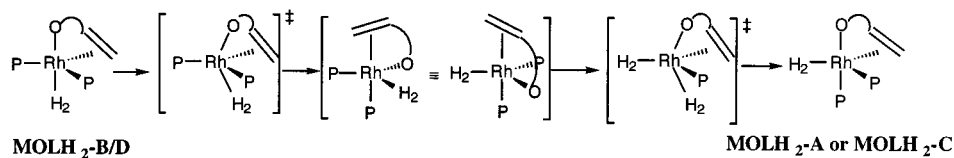


**Figure 11.** Double Berry pseudorotation process for **MOLH<sub>2</sub>** isomerization.

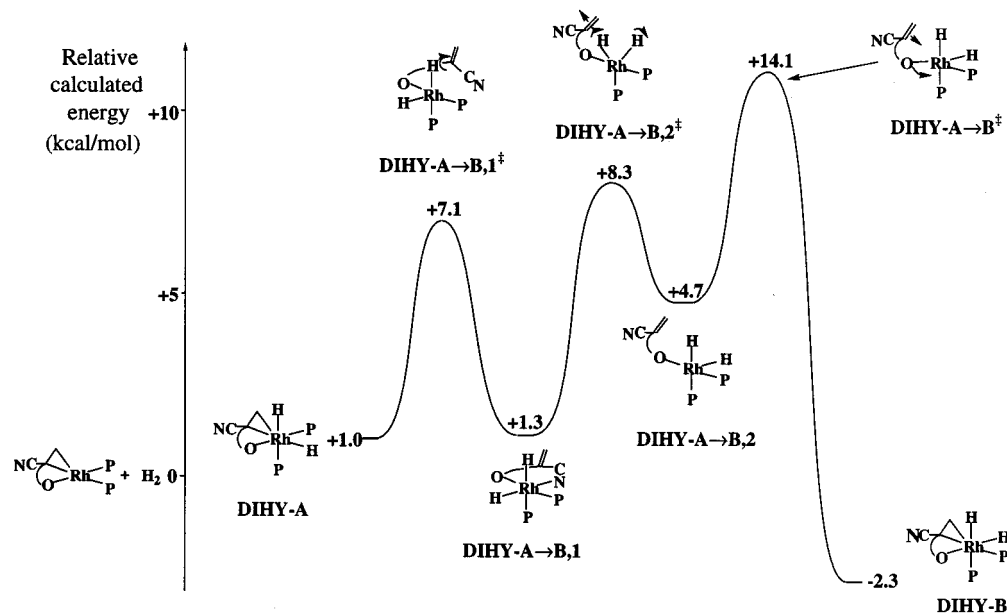


**Figure 12.** Mechanistic scheme for dihydride isomerization that interconverts **DIHY-A** and **DIHY-B**.

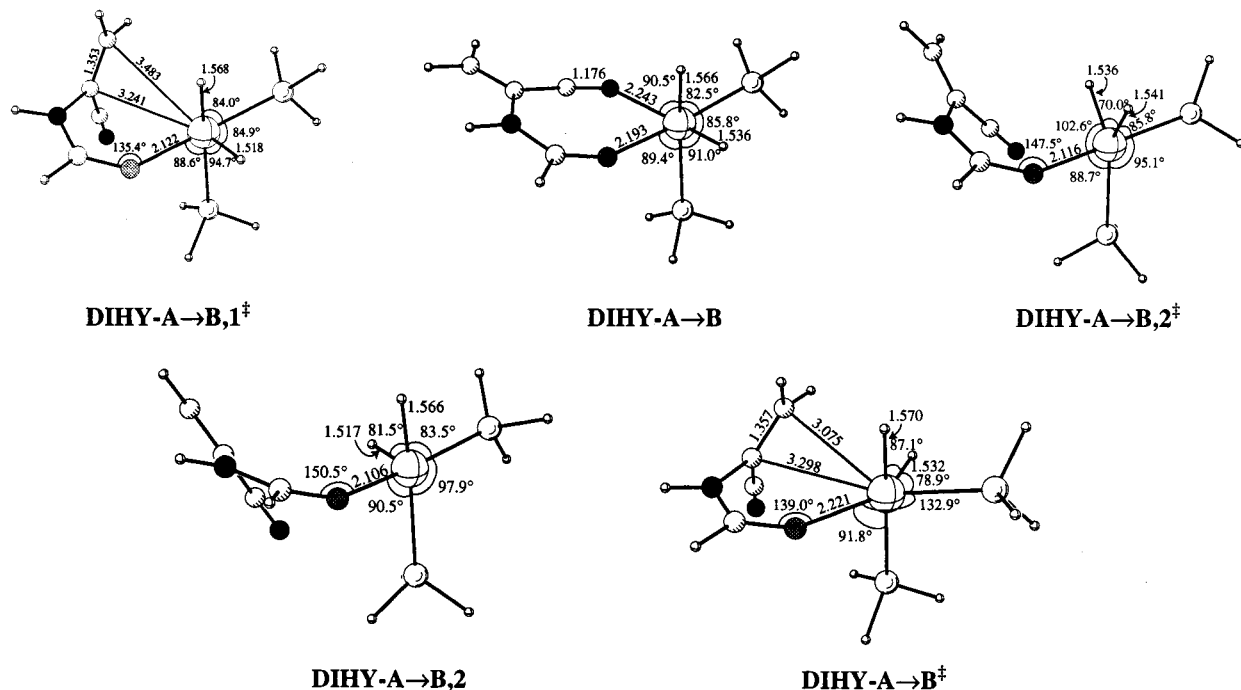


**Figure 13.** Structures along the three-step pathway for the interconversion of **DIHY-A**→**B**.

the nature of reaction transition states. To better interpret kinetic isotope effects (using H<sub>2</sub>, D<sub>2</sub>, and HD) that Landis and Brauch<sup>24</sup> and Brown and Parker<sup>26</sup> previously have measured for Rh-catalyzed enamide hydrogenation, we have computed kinetic and equilibrium isotope effects for selected transformations along the model **1** system pathways using the approach of Krogh-Jespersen et al.<sup>56</sup> In Table 3, the computed equilibrium and kinetic isotope effects for H<sub>2</sub> vs D<sub>2</sub> along the reaction pathway are shown. The formation of the molecular hydrogen

complexes has significant inverse equilibrium isotope effects (i.e., favoring formation of the D<sub>2</sub> adduct), ranging from 0.581 to 0.861. Further conversion of the molecular hydrogen complexes to dihydrides is accompanied by inverse equilibrium isotope effects for **DIHY-A** and **DIHY-C**. The computed reaction pathway suggests that the dihydride complexes are in rapid equilibrium with the Rh(I) complex **SQPL** and H<sub>2</sub>. The

(56) Abu-Hasanayn, F.; Krogh-Jespersen, K.; Goldman, A. S. *J. Am. Chem. Soc.* **1993**, *115*, 8019–8023.

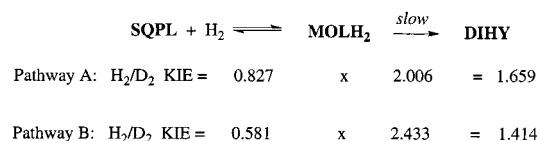
**Table 3.** Computed Equilibrium Isotope Effects (EIE), Forward Kinetic Isotope Effects (KIE), and Tunneling Corrections (TC) for H<sub>2</sub> vs D<sub>2</sub> along the Reaction Pathway

| transformation                | K (EIE) | k <sup>f</sup> (KIE) | TC <sup>a</sup> |
|-------------------------------|---------|----------------------|-----------------|
| SQPL → MOLH <sub>2</sub> -A   | 0.827   |                      |                 |
| SQPL → MOLH <sub>2</sub> -B/D | 0.581   |                      |                 |
| SQPL → MOLH <sub>2</sub> -C   | 0.861   |                      |                 |
| MOLH <sub>2</sub> -A → DIHY-A | 0.754   | 2.006                | 1.864           |
| MOLH <sub>2</sub> -B → DIHY-B | 1.070   | 2.433                | 1.269           |
| MOLH <sub>2</sub> -C → DIHY-C | 0.724   |                      |                 |
| MOLH <sub>2</sub> -D → DIHY-D | 1.045   |                      |                 |
| DIHY-A → ALHY-Aα              |         | 1.852                | 1.334           |
| DIHY-B → ALHY-Bα              |         | 1.610                | 1.096           |

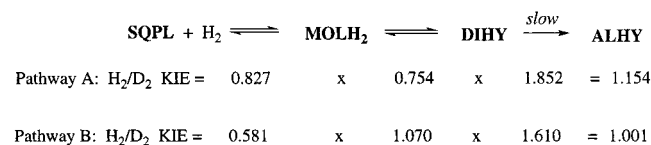
<sup>a</sup> Tunneling corrections to KIE calculations are presented but not factored into the forward kinetic isotope effects.

**Scheme 1**

H<sub>2</sub>/D<sub>2</sub> Kinetic Isotope Effect: Oxidative Addition = Turnover-limiting Step

**Scheme 2**

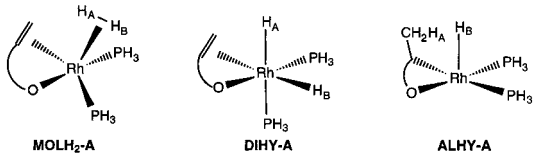
H<sub>2</sub>/D<sub>2</sub> Kinetic Isotope Effect: Insertion = Turnover-limiting Step



cumulative equilibrium isotope effects for these equilibria all are inverse: SQPL → DIHY-A = 0.623, SQPL → DIHY-B = 0.622, SQPL → DIHY-C = 0.623, and SQPL → DIHY-D = 0.607. These values are similar to previous experimental and computational<sup>56</sup> equilibrium isotope effects for the formation of transition metal dihydrides. In contrast to the inverse equilibrium isotope effects, the forward kinetic isotope effects for the formation of dihydrides are normal. As calculated in Scheme 1 with values from Table 3, if there were a rapid preequilibrium between the square planar complex (SQPL) and the molecular hydrogen complexes (MOLH<sub>2</sub>), the kinetic isotope effects for oxidative addition to form dihydrides would be substantial: SQPL → DIHY-A = 1.66 and SQPL → DIHY-B = 1.41. However, the experimentally measured isotope effects are small (1.0–1.2).

Our computations suggest that the kinetic model for enamide hydrogenation involves a rapid preequilibrium between the Rh(I) enamide adduct (SQPL) and the Rh(III) dihydrides (DIHY), followed by turnover-limiting insertion to form the alkyl hydrides (ALHY). Based on this prediction, the kinetic isotope effects for transformations of SQPL + H<sub>2</sub> to form ALHY-Aα and ALHY-Bα, as calculated in Scheme 2, are 1.154 and 1.001, respectively. Thus, the measured and computed H<sub>2</sub>/D<sub>2</sub> kinetic isotope effects for enamide hydrogenation support an insertion-limited pathway.

The catalytic reduction of enamides with HD yields interesting results.<sup>24,26</sup> The D is not distributed equally among the α and β positions of the product. Instead, there is a measured preference for D to occupy the α position over the β position by a factor of ca. 1.20–1.35. As shown in Table 4, we have computed equilibrium and kinetic isotope effects for various HD isomers along pathway A in the catalytic cycle. As with the H<sub>2</sub>/D<sub>2</sub> kinetic isotope effect, we have computed the HD/

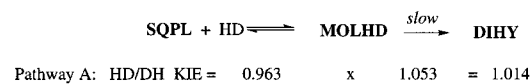
**Table 4.** Computed Equilibrium Isotope Effects (EIE), Forward Kinetic Isotope Effects (KIE), and Tunneling Corrections (TC) for Isomers Resulting from HD Addition along Pathway A


| transformation                | K <sub>H<sub>A</sub>D<sub>B</sub>}/K<sub>D<sub>A</sub>H<sub>B</sub></sub> (EIE)</sub> | k <sup>f</sup> <sub>H<sub>A</sub>D<sub>B</sub>}/k<sup>f</sup><sub>D<sub>A</sub>H<sub>B</sub></sub> (KIE)</sub> | TC <sup>a</sup> |
|-------------------------------|---------------------------------------------------------------------------------------|----------------------------------------------------------------------------------------------------------------|-----------------|
| SQPL-A → MOLH <sub>2</sub> -A | 0.963                                                                                 |                                                                                                                |                 |
| MOLH <sub>2</sub> -A → DIHY-A | 1.036                                                                                 | 1.053                                                                                                          | 1.066           |
| DIHY-A → ALHY-Aα              |                                                                                       | 1.600                                                                                                          | 1.320           |

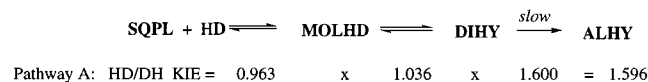
<sup>a</sup> Tunneling corrections to KIE calculations are presented but not factored into the forward kinetic isotope effects.

**Scheme 3**

HD/DH Kinetic Isotope Effect: Oxidative Addition = Turnover-limiting Step



HD/DH Kinetic Isotope Effect: Insertion = Turnover-limiting Step



DH isotope effect according to two scenarios, as shown in Scheme 3: turnover-limiting oxidative addition and turnover-limiting insertion.

From computations, it is clear that there is virtually no KIE or EIE for swapping H and D between alternate sites in the Rh dihydrides. This parallels the finding of Landis and Brauch that addition of HD to [Ir(dppe)(COD)]<sup>+</sup> has no KIE or EIE for formation of the two possible dihydride site isomers (dppe = 1,2-bis(diphenylphosphino)ethane).<sup>24</sup> The dominant influence on enamide reduction with HD is a large normal kinetic isotope effect for the insertion reaction to yield ALHY-Aα. Assuming that insertion is turnover-limiting, we compute a 1.596 preference for D to appear in the α position of the product, compared to the β position.

**Computations on a More Realistic Model.** A potential deficiency of ab initio computations performed with model ligands, such as PH<sub>3</sub>, is that the electronic effects of the PH<sub>3</sub> ligand are very different from those of the tertiary organophosphine ligands commonly used in catalysis. We have computed the energies of various intermediates for a catalyst containing a tertiary organophosphine ligand, model 2. The results of these computations are shown in Figure 14. Note that these results do not address kinetic differences between model 1 and model 2.

Overall, model 1 and model 2 yield similar results with no systematic differences other than the observation that the range of isomer energies for model 2 is greater than that of model 1. Presumably, the greater range for model 2 reflects differing combinations of the counterbalancing effects of increased electron richness with those of increased rigidity and steric bulk for the phosphine of model 2 relative to that of model 1. For example, one might anticipate<sup>52</sup> that all dihydride isomers (having formal oxidation state Rh(III)) would be more stabilized by the electron-rich tertiary phosphine (model 2) than by the PH<sub>3</sub> (model 1). For example, DIHY-B and DIHY-D isomers are stabilized for model 2 relative to model 1. In contrast,

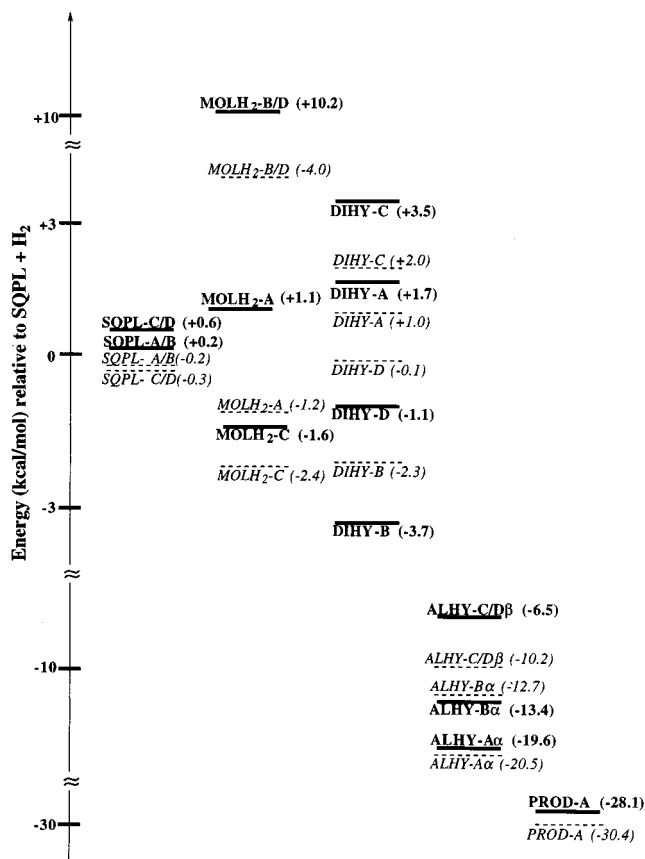


**Figure 14.** Comparison of the energies of intermediates along the reaction pathway for model **1** (italics) and model **2** (bold) complexes.

however, the **DIHY-A** and **DIHY-C** isomers are destabilized. Similarly, the alkyl hydride and molecular hydrogen intermediate isomers exhibit greater variability in energies for model **2** than for model **1**. Overall, although there are differences in the stabilities of intermediates for model **1** and model **2**, the changes are sufficiently small that it is likely the overall mechanistic features for the two systems are similar. However, a caveat is in order. It is likely that the sterically bulky ligands used in catalytic asymmetric reactions will perturb significantly the relative energies of various intermediates and transition states. These perturbations could result in different mechanistic pathways.

#### IV. Conclusions

**Overview of the Reaction Mechanism (Part 2).** If one does not consider pathway crossing (i.e., isomerizations among the A, B, C, and D pathways), the primary kinetic pathway for enamide hydrogenation is pathway A. Pathways B and D are excluded by virtue of the high kinetic barrier to formation of the molecular hydrogen intermediate, **MOLH<sub>2</sub>-B/D**. The very high kinetic barrier to insertion for pathway C precludes significant contribution of this pathway to product formation.

In principle, the high barrier to formation of **MOLH<sub>2</sub>-B/D** could be avoided by direct isomerization of either **MOLH<sub>2</sub>-A** or **MOLH<sub>2</sub>-C** to **MOLH<sub>2</sub>-B/D**. However, we have been unable to find a low-energy pathway for isomerization among these five-coordinate isomers by either a turnstile or a double Berry pseudorotation mechanism.

Isomerization among dihydride isomers could permit pathway crossing and lower overall reaction barriers. For example, isomerization of **DIHY-A** to **DIHY-B** could result in faster hydrogenation by replacing the 7.4 kcal/mol barrier to insertion

for **DIHY-A** with the 0.9 kcal/mol barrier to insertion for **DIHY-B**. We have found an isomerization pathway connecting **DIHY-A** and **DIHY-B**; the pathway involves dissociation of the coordinated C=C double bond, followed by a sequence of site isomerizations. The computed barrier for this pathway is 10.4 kcal/mol in the gas phase. Taken literally, this means that dihydride isomerization of **DIHY-A** to **DIHY-B** should be a rare event (frequency <1% at 298 K) relative to simple continuation along pathway A. However, steric influences and the presence of solvent and counteranion could alter these conclusions. Addressing these issues computationally will be the subject of future calculations.

**Comparison of Computational and Empirical Data for Enamide Hydrogenation.** The purpose of this work is to provide insights into the elementary processes of catalytic enamide hydrogenation that are not available by direct spectroscopic probes. The results of these computations are provocative. We suggest that (1) the kinetics of formation of molecular dihydrogen complexes play a critical role in determining the kinetic pathways, (2) dihydride complexes are true intermediates in the catalytic cycle, but only two of these are kinetically accessible, (3) one of the dihydride isomers undergoes insertion too slowly to play a significant role in catalysis, and (4) the turnover-limiting step is insertion of the alkene into a Rh-H bond. However, before discussing new insights gained from the computational results, we first address the consistency of the computed results with well-established empirical data. These empirical data include (1) the crystallographic structures of related enamide complexes, (2) the first-order dependence of the catalytic hydrogenation rate on dihydrogen pressure, (3) the failure to observe dihydrides by direct measurements involving normal dihydrogen, (4) the direct spectroscopic observation of a dihydride by PHIP (para-hydrogen-induced polarization) experiments, (5) the magnitudes of the apparent activation enthalpies of catalytic enamide hydrogenation, (6) the measured activation enthalpies for alkyl hydride reductive elimination, and (7) kinetic isotope effects involving H<sub>2</sub>, D<sub>2</sub>, and HD.

Are the structures of the computational models similar to crystallographically determined structures? As the data in Table I reveal, the overall geometric features of the model enamide complexes and crystallographically determined data are similar. One persistent shortcoming of the ab initio computations is the overestimation of Rh-P bond lengths by ca. 0.1 Å, although this is improved substantially through the use of large basis sets, such as Basis II. Despite this shortcoming, empirical trends such as the decreased Rh-P bond length trans to O vs that trans to the C=C double bond are reproduced in the computations.

Are the computed results consistent with the strictly first-order dependence<sup>46,57,58</sup> of non-asymmetric enamide hydrogenation rates on dihydrogen pressure? For all chelating bis-(phosphine)rhodium-catalyzed hydrogenations reported to date, the rate is strictly first-order in dihydrogen pressure up to ca. 100 atm. (Complexes with monophosphine ligands are commonly zero-order in dihydrogen pressure due to the stability of dihydride complexes with trans-disposed phosphines.) Our computational results are consistent with this empirical rate law. Let us consider reaction along pathway A, only. The computed potential energy surface suggests that the turnover-limiting step is insertion to form an alkyl hydride (**ALHY-Aα**) from a dihydride intermediate (**DIHY-A**). However, this step is preceded by an endergonic ( $\Delta G^\circ \approx 11$  kcal/mol, assuming a  $T\Delta S^\circ$

(57) Halpern, J.; Okrasinski, S. J. Unpublished results, 1981.

(58) Halpern, J.; Riley, D. P.; Chan, A. S. C.; Pluth, J. J. *J. Am. Chem. Soc.* **1977**, *99*, 8055–8057.

contribution of 10 kcal/mol) preequilibrium to form **DIHY-A** from  $H_2$  and **SQPL-A**. Partial saturation of this equilibrium, which would yield a non-first-order dependence of the catalytic reaction rate on  $H_2$  pressure, would require dihydrogen pressure greater than 1000 atm. Thus, the computed potential energy surface and the empirical rate law are mutually consistent.

A mechanism in which a rapid preequilibrium to form dihydride intermediates precedes turnover-limiting insertion is compatible with ortho–para- $H_2$  exchange data. Brown and co-workers<sup>59</sup> found that catalytic hydrogenation of enamides with para-enriched  $H_2$  did not lead to measurable interconversion of unreacted ortho and para- $H_2$ . This was interpreted as indicating that dihydrides were not formed reversibly. However, the critical factor determining the extent of ortho–para interconversion is the rate of the insertion relative to the rate of the nuclear triplet–singlet (ortho–para) transition in the dihydride. *As long as insertion occurs faster than the interconversion between ortho and para spin states,  $H_2$  will be consumed more rapidly than ortho–para equilibration.* We can estimate the rate of ortho–para interconversion in the dihydride intermediate from the longitudinal spin relaxation time,  $T_1$ , in a vanishingly small external magnetic field. Certainly,  $T_1$  is on the order of magnitude of 1 s at room temperature, similar to  $T_1$  for water in the low-field limit. In contrast, the pseudo-first-order insertion rate must be *at least* as large as the catalytic turnover frequency. At 100 atm pressure of  $H_2$ , the hydrogenation of methyl (*Z*)- $\alpha$ -acetamidocinnamate with the catalyst precursor  $[Rh(dppe)(NBD)]^+$  yields turnover half-lives on the order of 30 ms.<sup>57</sup> Thus, a mechanism in which  $H_2$  addition is rapid and reversible relative to rate-determining insertion is consistent with the experimental observation of no ortho–para- $H_2$  interconversion during catalytic hydrogenation.

Should one observe dihydrides directly under hydrogenation conditions? Using NMR methods, mononuclear dihydrides of Rh complexes containing chelating phosphines are not observed under modest pressures of  $H_2$ . For example, the  $^1H$  NMR of  $[Rh(dppe)(methanol)_2]^+$  under 10 atm of dihydrogen does not exhibit measurable resonances for  $[Rh(H)_2(dppe)(methanol)_2]^+$ .<sup>60</sup> These results are consistent with the generally endergonic nature of the dihydrogen oxidative addition reaction to cationic complexes of Rh containing chelate phosphine ligands, as revealed by our ab initio computations.

Is the direct observation of a dihydride intermediate under PHIP conditions consistent with computational data? The NMR signal of metal hydrides formed from para-enriched  $H_2$  can exhibit signal enhancements as high as  $10^5$ . Recently, Bargon and co-workers<sup>61</sup> have reported the direct observation of a dihydride intermediate using the PHIP technique. Under PHIP conditions, the hydrogenation of itaconic acid with a cationic bis(phosphite)Rh catalyst results in an NMR signal attributable to a dihydride intermediate. This dihydride is not detected using standard NMR methods. Because the PHIP enhancements are so large, observation of the steady-state concentration corresponding to 0.01% of the total catalyst concentration certainly is possible. Such steady-state concentrations are consistent with endergonic formation of dihydride intermediates, as revealed by our computations.

Are empirical estimates of dihydrogen activation enthalpies consistent with our computational results? Empirical data<sup>18,46</sup> on the Rh-catalyzed hydrogenation of enamides yield apparent

activation enthalpies in the range of 7–10 kcal/mol. Previously these were interpreted as enthalpies of activation for the oxidative addition reaction. Neglecting zero-point energy and vibrational excitation contributions (which are on the order of the reliability of the computed energies), we estimate  $\Delta H^\ddagger \approx 8.4$  kcal/mol for pathway A. Empirical values of  $T\Delta S^\ddagger$  for the turnover-limiting step are estimated to be ca. 8.0 kcal/mol, which is roughly consistent with the value of 10 kcal/mol that we approximate for a bimolecular process. Given the differences in the actual systems studied empirically and computationally, the apparent activation parameters are in remarkably good agreement with computation. As a cautionary note, it should be pointed out that the computed activation parameters for the oxidative addition step along pathway A ( $\Delta H^\ddagger \approx 5.5$  kcal/mol) also are similar to the empirical values. Therefore, the magnitudes of the observed and calculated activation enthalpies are too close to conclusively discriminate between alkene insertion and oxidative addition as the rate-limiting step.

Are the computed results consistent with experimental trapping of the alkyl hydride intermediate at low temperatures ( $< -40$  °C)? The temperature dependence of the relative rates of reductive elimination and alkene insertion is controlled by the differences in the activation enthalpies for the two steps. Experimentally it is found that hydrogenation of enamide complexes similar to **SQPL-A/B** yield stable alkyl hydrides at low temperature. The structures proposed for these alkyl hydrides are similar to those of **ALHY-A $\alpha$**  but with a solvent, such as methanol, occupying the coordination site trans to the Rh–H bond. Importantly, we predict that the nitrile group and the hydride ligand are positioned on opposite sides of the P–Rh–P metal plane, similar to the arrangement determined by Brown and Maddox<sup>62</sup> for the Ir alkyl hydride formed initially upon hydrogenation of the minor diastereomer of  $[Ir(DIPAMP)(methyl-\alpha\text{-acetamidocinnamate})]^+$ . Empirical measurements<sup>57,63</sup> for the Rh enamide systems yield apparent activation enthalpies for reductive elimination in the range of 15–20 kcal/mol. These values, which are sensitive to the nature of the ligand occupying the coordination position trans to the Rh–H bond, agree well with the computed activation enthalpy of 15.7 kcal/mol. Furthermore, the high exothermicity of alkyl hydride formation from a dihydride intermediate (ca.  $-21$  kcal/mol) dictates that alkyl hydride formation is irreversible, in agreement with experimental data.<sup>24</sup>

Do computations provide insight into the origin of observed isotope effects? Previous measurements of the kinetic isotope effect,<sup>24,26</sup>  $H_2$  vs  $D_2$ , for enamide hydrogenation yielded small, normal values in the range of 1–1.2:1. A different kind of isotope effect, the partitioning of HD isotopes among the  $\alpha$  and  $\beta$  positions of the amino acid product, exhibits a preference for H addition to the  $\beta$  position over the  $\alpha$  position by a ratio of 1.2–1.35:1.<sup>24,26</sup> For a given combination of catalyst and enamide, the HD partitioning ratio is always greater than the kinetic ratio for  $H_2$  vs  $D_2$ . Based on analysis of the data presented in Tables 3 and 4, computed values for the kinetic isotope effect clearly differentiate between a mechanism in which oxidative addition along pathway A is turnover-limiting ( $k(H_2):k(D_2) = 1.66:1$ ) and one in which insertion is turnover-limiting ( $k(H_2):k(D_2) = 1.15:1$ ). Similar differentiation is obtained for the partitioning of HD; pathway A with turnover-limiting insertion yields a larger ratio ( $H_\alpha:H_\beta = 1.6$ ) than for pathway A with turnover-limiting oxidative addition ( $H_\alpha:H_\beta =$

(59) Brown, J. M.; Canning, L. R.; Downs, A. R.; Forster, A. M. *J. Organomet. Chem.* **1983**, 255, 103–111.

(60) Halpern, J.; Landis, C. R. Unpublished results, 1983.

(61) Harthun, A.; Kadyrov, R.; Selke, R.; Bargon, J. *Angew. Chem., Int. Ed. Engl.* **1997**, 36, 1103–1005.

(62) Brown, J. M.; Maddox, P. J. *J. Chem. Soc., Chem. Commun.* **1987**, 1276–1278.

(63) Chan, A. S. C.; Halpern, J. *J. Am. Chem. Soc.* **1980**, 102, 838–840.

1.0). Overall, the trends in computed kinetic isotope effects are more consistent with experimental isotope effects if the turnover-limiting step is alkene insertion. We believe that this provides the most compelling data for a mechanism involving a rapid preequilibrium to form a dihydride followed by turnover-limiting insertion of the alkene into a Rh–H bond.

**General Implications for Catalytic Asymmetric Hydrogenation.** The most striking feature of this work is the critical role played by molecular H<sub>2</sub> complexes controlling kinetic access to isomeric reaction pathways. To the best of our knowledge, these computations provide the first evidence that molecular H<sub>2</sub> complexes may represent more than a shallow “pothole” along the potential energy surface to oxidative addition. However, we note that Crabtree and co-workers’<sup>64</sup> proposed mechanism of H<sub>2</sub> oxidative addition at Ir centers anticipated these results remarkably well. Crabtree and co-workers proposed that observed stereochemical isomer distributions correlate with stabilities of five-coordinate molecular H<sub>2</sub> complexes. Most notably, the slow rate of formation of complexes with H<sub>2</sub> in the axial position (analogous to **MOLH<sub>2</sub>-B/D**) was anticipated and attributed to slow Berry pseudorotation. Similarly, we find that there is no low-energy pathway to molecular H<sub>2</sub> complexes with H<sub>2</sub> in the axial position either via isomerization from another site isomer or by direct reaction with H<sub>2</sub>. As a result, two of the four isomeric pathways for catalytic hydrogenation are precluded. Because this rate discrimination among isomeric pathways occurs in a sterically uncongested model system, we conclude that its origin is electronic rather than steric.

A second striking feature of this work is the identification of insertion, not oxidative addition, as the turnover-limiting step (and, by extrapolation, the enantiodetermining step in catalytic asymmetric hydrogenation). Essentially all previous work has assumed that oxidative addition is turnover-limiting. An important implication of this work is that design of highly selective ligand structures may need to focus on the structures of insertion transition states rather than oxidative addition transition states.<sup>65,66</sup> However, features of the computed potential energy surface may change significantly as more realistic ligands, substrates, and solvents are included. Future work, which is already in progress, will focus on combined QM/MM approaches to modeling the potential energy surfaces of the eight isomeric pathways arising from asymmetric hydrogenation reactions.

(64) Burk, M. J.; McGrath, M. P.; Wheeler, R.; Crabtree, R. H. *J. Am. Chem. Soc.* **1988**, *110*, 5034.

(65) Leitner, W.; Brown, J. M.; Brunner, H. *J. Am. Chem. Soc.* **1993**, *115*, 152–159.

## V. Summary

The mechanism of non-asymmetric Rh-catalyzed hydrogenation of enamides has been probed by DFT computations of a simple model catalyst, [Rh(PH<sub>3</sub>)<sub>2</sub>( $\alpha$ -formamidoacrylonitrile)]<sup>+</sup>. The potential energy surfaces generated for four isomeric reaction pathways demonstrate the critical role of molecular H<sub>2</sub> complexes in discriminating the kinetics of the various pathways. According to these computations, the insertion of alkene into a Rh–H bond constitutes the turnover-limiting step in the catalytic process. A general mechanism derived from this work effectively accounts for numerous empirical data from the empirical rate law, kinetic isotope effects, ortho–para-H<sub>2</sub> interconversion, and PHIP measurements. In addition, this work demonstrates the power of ab initio methods for elucidating mechanistic aspects of catalytic reactions that are difficult to probe experimentally. We are continuing this work with an emphasis on the application of hybrid QM/MM methods on chiral hydrogenation catalysts and elucidation of the origins of enantiodifferentiation. These results, which demonstrate striking similarities between the mechanism found in this study and that for the larger asymmetric catalysts, will be the subject of a future publication.

**Acknowledgment.** This work was supported by the National Science Foundation (CHE-9618497) and the Wisconsin Alumni Research Foundation. This work was partially supported by the National Center for Supercomputer Applications under CHE970025N and utilized the computer system SGI CRAY ORIGIN2000 at the National Center for Supercomputer Applications. The authors are indebted to one of the reviewers, who commented on the manuscript in immense detail.

**Supporting Information Available:** Tables of Cartesian coordinates and computed vibrational frequencies for all fully optimized intermediate and transition-state structures (PDF). This material is available free of charge via the Internet at <http://pubs.acs.org>.

JA991606U

(66) We note that turnover-limiting alkene insertion may help to explain Brown and Leitner’s observation that enamide reduction with formic acid yields enantioselectivities that are nearly identical to those obtained by reduction with dihydrogen, even though dihydrogen is not an intermediate in the formic acid reductions.